Optimal Control of Multilevel DAB Converters for Soft-Switching and Minimum Current Stress

Chaochao Song, *Member, IEEE*, Ariya Sangwongwanich, *Member, IEEE*, Yongheng Yang, *Senior Member, IEEE*, and Frede Blaabjerg, *Fellow, IEEE*

***Abstract*—Multilevel dual-active-bridge (DAB) dc–dc converters offer higher voltage-blocking capability and larger step-up ratios, as well as increased number of degrees of freedom (DoFs) compared with the traditional two-level DAB converter. Thus, it has potential to be used in medium-voltage dc systems. However, the control complexity of the multi-level DAB converters also increases along with the number of DoFs. When soft-switching is considered as an optimization objective together with other performance indices (e.g., peak or root-mean-square values of the inductor current), the analytical solutions will be difficult to derive due to the increased number of control variables and complicated soft-switching constraints. To address this issue and improve the efficiency of the DAB converter, this article proposes a control strategy for a multilevel DAB converter to achieve both soft-switching and minimum-current-stress simultaneously. The analytical solutions are calculated by improved Karush–Kuhn–Tucker (KKT) conditions, where the numerical solutions are used to locate the operating modes and determine the zero-voltage-switching (ZVS) boundaries. This can simplify the Lagrangian function and inequality constraints, and then, the analytical solutions can be obtained by the simplified KKT conditions. In addition, a comprehensive comparison between the quasi-ZVS and strict-ZVS control is carried out, so that the converter efficiency, implementation complexity, and smooth transition between different power levels can be compromised for practical applications. Finally, the performances of the proposed control strategy in terms of current stress minimization and soft-switching operation are validated by experimental tests.**

***Index Terms*—Dual-active-bridge (DAB) converters, minimum current stress (MCS), multilevel converters, optimal control strategy, soft-switching.**

I. Introduction

TWO-THREE (2/3)-level dual-active-bridge (DAB) converter (also referred to as 5-level DAB converter in [1]), as shown in Fig. 1, is a promising dc–dc converter interlinking medium-voltage dc (MVdc) and low-voltage dc systems, e.g., energy storage systems, large-scale photovoltaic plants, electric vehicles, and microgrids with an MVdc structure [2], [3], [4], [5]. This is because, in addition to the advantages of the traditional two-level DAB converter, such as high power density and efficiency, galvanic isolation, soft-switching capability, and bidirectional power-flow capability, the three-level neutral-point-clamped (NPC) topology can also increase the voltage-blocking capability of the dc–dc converter [6], [7], [8], [9]. Furthermore, the increased number of degrees of freedom (DoFs) in the control for the multilevel topology due to an increased number of possible switching combinations can be used to optimize the performances of the DAB converter, e.g., improving the efficiency.

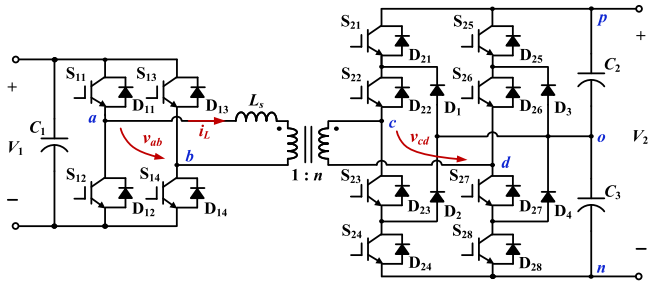

Fig. 1. 2/3-level DAB converter: V_1 and V_2 are the DC-link voltages, v_{ab} and v_{cd} are the AC voltages besides the isolated transformer, L_s is the inductor composed of the auxiliary inductor and the leakage inductance of the transformer, i_L is the inductor current, and $1:n$ is the turns ratio of the transformer.

In terms of control, multiphase-shift (MPS) control methods are generally employed to regulate the transferred power of the DAB converters to enhance the efficiency, especially when the two dc-link voltages (i.e., V_1 and V_2 in Fig. 1) are not matched (i.e., the voltage conversion ratio is away from unity) [10], [11]. For a certain reference operating condition, there are various combinations of the control variables (i.e., phase-shift angles and duty cycles), which can meet the requirements. However, the performances of the DAB converters will vary under different combinations of the control variables. Thus, many optimal control strategies have been proposed in the literature for optimum combinations of the control variables, e.g., minimizing the peak or root-mean-square (rms) values of the inductor current, reducing the power losses, or achieving soft-switching operation [5], [12], [13], [14], [15], [16], [19], [20], [21], [22], [23], [24].

There are generally two types of solutions that are used to do so, i.e., numerical solutions and analytical solutions. Compared with the numerical solutions, where the optimal

Manuscript received 19 December 2023; accepted 30 January 2024. Date of publication 5 February 2024; date of current version 20 March 2024. This work was supported in part by the research project Reliable Power Electronic based Power Systems (REPEPS) by the Velux Foundations under Grant 00016591 and in part by the National Natural Science Foundation of China under Grant 52107212. Recommended for publication by Associate Editor S. K. Mazumder. *(Corresponding author: Yongheng Yang.)*

Chaochao Song, Ariya Sangwongwanich, and Frede Blaabjerg are with the AAU Energy, Aalborg University, 9220 Aalborg, Denmark (e-mail: chso@energy.aau.dk; ars@energy.aau.dk; fbl@energy.aau.dk).

Yongheng Yang is with the College of Electrical Engineering, Zhejiang University, Hangzhou 310027, China (e-mail: yang_yh@zju.edu.cn).

Color versions of one or more figures in this article are available at https://doi.org/10.1109/TPEL.2024.3362051.

Digital Object Identifier 10.1109/TPEL.2024.3362051

solutions should be precalculated offline, and then, stored in the microcontrollers by a look-up table [5], [20], [21], the analytical solutions are favorable in practical applications, especially when the dc-link voltages and/or transferred power change in a wide range [22]. That is because the control variables can be regulated online along with the changed operating parameters. Analytical solutions have been widely presented in the literature, aiming at reducing the peak or rms values of the inductor current [12], [13], [14]. Furthermore, several control strategies for achieving both zero-voltage-switching (ZVS) and current stress minimization simultaneously were proposed based on the analytical solutions [15], [16], [17], [18]. However, all the above control strategies were developed based on the two-level DAB converter. As for the multilevel DAB converters, most of the prior-art control strategies employed the numerical solutions due to the increased number of control variables and complicated operating constraints [5], [19], [20], [21]. Yet, a minimum-current-stress (MCS) control strategy was proposed based on the analytical solutions, which are obtained based on the Karush–Kuhn–Tucker (KKT) conditions and numerical-solution analysis [22]. Nevertheless, the soft-switching was not considered as a control objective in this control strategy. Thus, the inherent soft-switching capability of the DAB converter was not utilized, which limits the efficiency improvement of the control strategy. Furthermore, the optimization approach used in [22] cannot solve the optimization problem with ZVS constraints directly, because within a certain operating mode, the optimal solutions may locate at different ZVS boundaries, and thus, the expressions of the optimal solutions are different for a certain operating mode under various power levels. Only if the ZVS boundaries can be identified, the optimal solutions can be calculated by the KKT conditions. However, this issue have not been addressed in previous literature. It is evident that when both the two control objectives, i.e., current stress minimization and soft-switching, are considered in an optimal control, the analytical solutions are challenging to be obtained due to more complicated inequality constraints in the optimization problem. This is the reason why the prior-art control strategies for the multilevel DAB converters have only considered a single optimization objective, e.g., current stress/rms current minimization or ZVS operation [5], [20], [21], [22], [23], [24].

In order to improve the efficiency of the DAB converter to a greater extent, this article proposes a control strategy, which can simultaneously reduce the conduction and switching losses for the 2/3-level DAB converter, where the conduction losses can be decreased by minimizing the peak value of the inductor current, and the switching loss reduction can be achieved by the soft-switching operation [16]. The operating modes, which are able to achieve ZVS for all the switches are derived. Subsequently, the ZVS constraints, transferred power models, and current stress models for all the operating modes are analyzed. Accordingly, the optimal analytical solutions for minimizing the current stress and achieving soft-switching are obtained by improved KKT conditions. The main contributions of this article can be summarized as follows.

1) An improved KKT-condition-based approach is proposed to obtain the analytical solutions for the multilevel DAB converter under MPS control, where numerical solutions are used to locate the operating modes and determine the ZVS boundaries to simplify the calculation for analytical solutions. This can simplify the Lagrangian function and inequality constraints in the optimization problem, and then, the analytical solutions can be obtained by the simplified KKT conditions.
2) A comprehensive comparison is carried out on strict-ZVS and quasi-ZVS control in terms of power range, soft-switching region, current stress, and implementation complexity, which provides a benchmark for choosing certain soft-switching control strategy after compromising the efficiency and feasibility for the DAB converters with different power components (e.g., insulated gate bipolar transistor (IGBT) or MOSFET).
3) A generic closed-loop control structure is designed, which can be used to the condition where the control variables are not monotonically changed along with the transferred power. In addition, the current sensor is not needed, and thus, the hardware cost and control complexity can be reduced.
4) With the above improved techniques, an optimal control strategy combining both the MCS and soft-switching operation for the multilevel DAB converter is proposed. Therefore, both the conduction and switching losses can be reduced, and the converter efficiency can be further enhanced.

The rest of this article is organized as follows. The ZVS constraints, transferred power models, and current stress models for various operating modes are discussed in Section II. The optimal control strategies to achieve soft-switching and MCS are proposed in Section III. A comparison between the quasi-ZVS and strict-ZVS control strategies, as well as the closed-loop control structure is demonstrated in Section IV. Experimental tests are carried out to validate the performance of the proposed control strategy in Section V. Finally, Section VI concludes this article.

II. ZVS Analysis for 2/3-Level DAB Converter

A. Basic Characteristics

Fig. 2 shows a typical MPS control method for the 2/3-level DAB converter, where four control variables are applied to control the power flow and to optimize the performance, e.g., efficiency. D_0 is the outer phase-shift ratio between the two bridges, i.e., the gate pulses between S_{21} and S_{11}, D_1 and D_2 are the inner phase-shift ratios of the two-side bridges, and D denotes the duty-cycle ratio (i.e., $0 \leq D \leq 1$). In addition, T_{hs} is half of a switching period.

The waveform of the voltage v_{ab} will not change regardless of whether the gate pulse of S_{11} leads or lags behind that of S_{14} (i.e., D_1 is positive or negative). A similar condition occurs between the voltage v_{cd} and the polarity of D_2. Therefore, in order to simplify the analysis, the ranges of the two inner phase-shift ratios are defined as $0 \leq D_1 \leq 1$ and $0 \leq D_2 \leq 1$. On the other

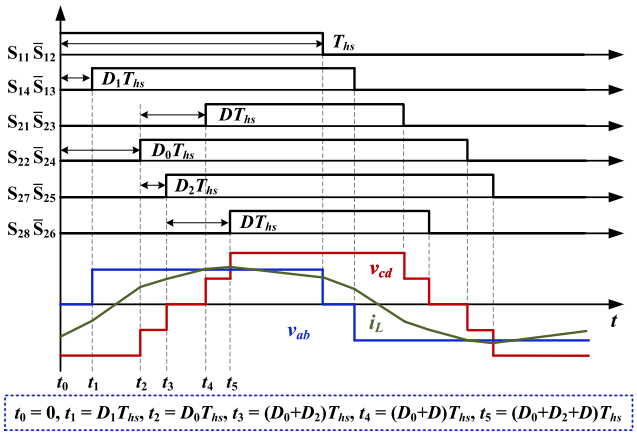

Fig. 2. Typical MPS control method for the 2/3-level DAB converter.

hand, the polarity of the outer phase-shift ratio D_0 will affect the inductor current i_L due to

$$\frac{di_L(t)}{dt} = \frac{v_{ab}(t) - v_{cd}(t)/n}{L_s} \tag{1}$$

and thus, further affecting the transferred power due to

$$P = \frac{1}{T_{hs}} \int_0^{T_{hs}} v_{ab}(t) i_L(t) dt. \tag{2}$$

Therefore, D_0 is defined as $-1 \le D_0 \le 1$. In addition, the waveform of v_{cd} will be the same for the conditions of $D_2 < D$ and $D_2 > D$. Thus, the transferred power range and other performances (e.g., current stress) will not be affected by the phase relationships between D_2 and D. In summary, the ranges of the control variables are defined as

$$\begin{cases} 0 \le D_1 \le 1, 0 \le D_2 \le 1, 0 \le D \le 1 \\ -1 \le D_0 \le 1 \\ D_2 \le D. \end{cases} \tag{3}$$

B. ZVS Constraints and Operating Modes

To achieve ZVS operation for a power switch, during the dead time before the rising edge of its gate pulse, there should be a minimal current to provide a discharging path for the output capacitor of the switch. After the capacitor is fully discharged, the switch can be turned ON in the ZVS state [16], [22]. Therefore, the unified ZVS constraints for all switches in both bridges can be obtained as [24], [25], [26]

$$\begin{cases} \frac{1}{2}L_s I_L^2(t_i) \ge 2 \cdot \frac{1}{2}C_{p1}V_1^2, & \text{Two-level full bridge} \\ \frac{1}{2}L_s I_L^2(t_j) \ge 4 \cdot \frac{1}{2}C_{p2}\left(\frac{V_2}{2}\right)^2, & \text{NPC bridge} \end{cases} \tag{4}$$

where C_{p1} and C_{p2} are the output capacitors of the switches in the two-side bridges, and $I_L(t_i)$ ($i = 0$ and 1) and $I_L(t_j)$ ($j = 2, 3, 4$, and 5) are the instantaneous inductor currents when the switches in the two-level bridge and NPC bridge are turned ON, respectively. Furthermore, the polarity of the instantaneous inductor current should be opposite to that of the switch voltage (e.g., from the emitter to the collector for IGBTs). Considering the required polarity of instantaneous inductor currents, the ZVS constraints for all the switches are obtained as

$$\begin{cases} I_L(t_i) \le -\sqrt{2C_{p1}V_1^2/L_s}, & i = 0, 1 \\ I_L(t_j) \ge \sqrt{C_{p2}V_2^2/L_s}, & j = 2, 3, 4, 5 \end{cases} \tag{5}$$

where $I_L > 0$ indicates that the current flows from the two-level full bridge to the NPC bridge, and vice versa.

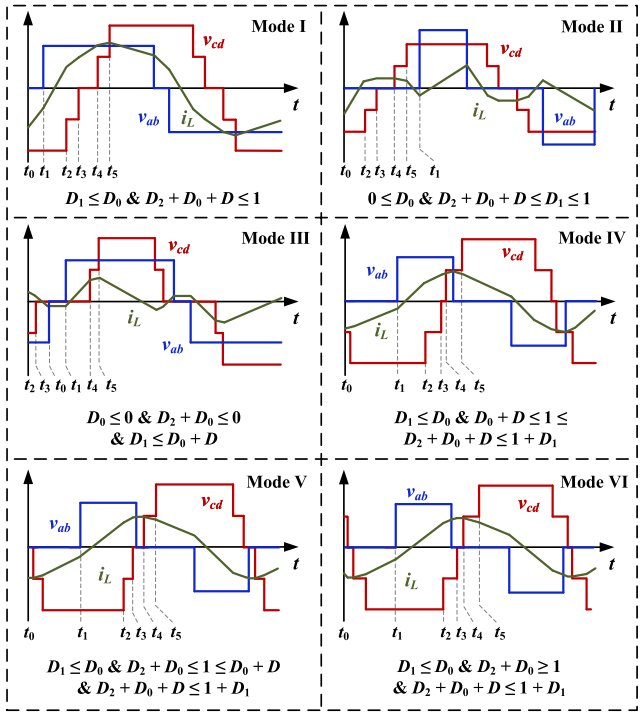

Fig. 3. Operating modes which can achieve ZVS operation of the 2/3-level DAB converter.

According to the above constraints, the operating modes, which are able to achieve ZVS for all switches can be obtained, as shown in Fig. 3, and they are defined as Modes I–VI based on different relationships among the control variables (i.e., mode constraints). It should be noted that Mode II can achieve ZVS only under the condition of $k > 1$, where k is the voltage conversion ratio, defined as $k = nV_1/V_2$. Otherwise, the ZVS constraints for the two-side switches cannot be satisfied at the same time. Similarly, Mode III can achieve ZVS only under the condition of $0 < k \le 1$. On the other hand, the other modes, i.e., Modes I, IV, V, and VI, can be applied for both conditions (i.e., $0 < k \le 1$ and $k > 1$). According to (1) and the symmetry of the inductor current i_L, the expressions of the instantaneous inductor currents when the switches are turned ON can be calculated, and thus, the ZVS constraints under each operating mode can be obtained, as given in Table I, where $I_N = V_2 T_{hs}/(4nL_s)$, and I_{ZVS1} and I_{ZVS2} indicate the minimal inductor currents in the ZVS constraints, i.e.,

$$\begin{cases} I_{ZVS1} = \sqrt{2C_{p1}V_1^2/L_s} \\ I_{ZVS2} = \sqrt{C_{p2}V_2^2/L_s}. \end{cases} \tag{6}$$

In order to achieve ZVS for all the switches, the ZVS constraints given in Table I should be satisfied in the proposed control strategy.

TABLE I
ZVS CONSTRAINTS FOR VARIOUS OPERATING MODES

Modes	ZVS constraints
I	$I_L(t_0)=2I_N(kD_1-D_2-2D_0-D-k+1)\le -I_{ZVS1}$, $I_L(t_1)=2I_N((k+2)D_1-D_2-2D_0-D-k+1)\le -I_{ZVS1}$ $I_L(t_2)=2I_N(-kD_1-D_2+2kD_0-D-k+1)\ge I_{ZVS2}$, $I_L(t_3)=2I_N(-kD_1+2kD_0+(2k-1)D-k+1)\ge I_{ZVS2}$ $I_L(t_4)=2I_N(-kD_1+2kD_2+2kD_0-D-k+1)\ge I_{ZVS2}$, $I_L(t_5)=2I_N(-kD_1+(2k-1)D_2+2kD_0+(2k-1)D-k+1)\ge I_{ZVS2}$
II	$I_L(t_0)=2I_N(kD_1-D_2-2D_0-D-k+1)\le -I_{ZVS1}$, $I_L(t_1)=2I_N((k-2)D_1+D_2+2D_0+D-k+1)\le -I_{ZVS1}$ $I_L(t_2)=I_L(t_5)=2I_N(kD_1-D_2-D-k+1)\ge I_{ZVS2}$, $I_L(t_3)=I_L(t_4)=2I_N(kD_1-D-k+1)\ge I_{ZVS2}$
III	$I_L(t_0)=I_L(t_1)=2I_N(kD_1-D-k+1)\le -I_{ZVS1}$, $I_L(t_2)=2I_N(kD_1-2kD_0-D-k+1)\ge I_{ZVS1}$ $I_L(t_3)=2I_N(kD_1-2kD_2-2kD_0-D-k+1)\ge I_{ZVS2}$, $I_L(t_4)=2I_N(-kD_1+2kD_0+(2k-1)D-k+1)\ge I_{ZVS2}$ $I_L(t_5)=2I_N(-kD_1+(2k-1)D_2+2kD_0+(2k-1)D-k+1)\ge I_{ZVS2}$
IV	$I_L(t_0)=2I_N(kD_1-D_0-k)\le -I_{ZVS1}$, $I_L(t_1)=2I_N((k+2)D_1-D_2-2D_0-D-k+1)\le -I_{ZVS1}$ $I_L(t_2)=2I_N(-kD_1-D_2+2kD_0-D-k+1)\ge I_{ZVS2}$, $I_L(t_3)=2I_N(-kD_1+2kD_2+2kD_0-D-k+1)\ge I_{ZVS2}$ $I_L(t_4)=2I_N(-kD_1+2kD_0+(2k-1)D-k+1)\ge I_{ZVS2}$, $I_L(t_5)=2I_N(-kD_1-D_2-D+k+1)\ge I_{ZVS2}$
V	$I_L(t_0)=2I_N(kD_1+D-k-1)\le -I_{ZVS1}$, $I_L(t_1)=2I_N((k+2)D_1-D_2-2D_0-D-k+1)\le -I_{ZVS1}$ $I_L(t_2)=2I_N(-kD_1-D_2+2kD_0-D-k+1)\ge I_{ZVS2}$, $I_L(t_3)=2I_N(-kD_1+2kD_2+2kD_0-D+k+1)\ge I_{ZVS2}$ $I_L(t_4)=2I_N(-kD_1-D+k+1)\ge I_{ZVS2}$, $I_L(t_5)=2I_N(-kD_1-D_2-D+k+1)\ge I_{ZVS2}$
VI	$I_L(t_0)=2I_N(kD_1-D_2+D_0+D-k-2)\le -I_{ZVS1}$, $I_L(t_1)=2I_N((k+2)D_1-D_2-2D_0-D-k+1)\le -I_{ZVS1}$ $I_L(t_2)=2I_N(-kD_1-D_2+2kD_0-D-k+1)\ge I_{ZVS2}$, $I_L(t_3)=I_L(t_4)=2I_N(-kD_1-D+k+1)\ge I_{ZVS2}$ $I_L(t_5)=2I_N(-kD_1-D_2-D+k+1)\ge I_{ZVS2}$

TABLE II
NORMALIZED TRANSFERRED POWER FOR ALL THE OPERATING MODES

Modes	Normalized peak current P_o
I	$2(-D_1^2-D_2^2-2D_0^2-D^2+D_1D_2+2D_1D_0+D_1D-2D_2D_0-2D_0D-D_2D-D_1+D_2+2D_0+D)$
II	$2(D_1^2-D_1D_2-2D_1D_0-D_1D-D_1+D_2+2D_0+D)$
III	$2(-D^2+D_1D-D_2D-2D_0D-D_1+D_2+2D_0+D)$
IV	$2(-D_1^2-0.5D_2^2-1.5D_0^2-0.5D^2+D_1D_2+2D_1D_0+D_1D-D_2D_0-D_0D-D_1+D_0+0.5)$
V	$2(-D_1^2-0.5D_2^2-D_0^2+D_1D_2+2D_1D_0+D_1D-D_2D-D_1-D+1)$
VI	$2(-D_1^2-0.5D_0^2+D_1D_2+2D_1D_0+D_1D-D_1-D_2-D_0-D+1.5)$

TABLE III
NORMALIZED PEAK CURRENT FOR ALL THE OPERATING MODES UNDER VARIOUS CONDITIONS

Modes	Normalized peak current i_o		
	$k>1$	$0.5<k\le 1$	$0<k\le 0.5$
I	$2\left[-kD_1+D_2+2D_0+D+k-1\right]$	$2\left[-kD_1+(2k-1)(D_2+D)+2kD_0-k+1\right]$	$2\left[-kD_1+2kD_0+(2k-1)D-k+1\right]$
II		–	–
III	–	$2\left[-kD_1+(2k-1)(D_2+D)+2kD_0-k+1\right]$	$2\left[-kD_1+2kD_0+(2k-1)D-k+1\right]$
IV	$2\left[-kD_1+D_0+k\right]$	$2\left[-kD_1+D_0+k\right]$	$2\left[-kD_1+2kD_0+(2k-1)D-k+1\right]$
V	$2\left[-kD_1-D+k+1\right]$	$2\left[-kD_1-D+k+1\right]$	$2\left[-kD_1-D+k+1\right]$
VI			

C. Transferred Power and Current Stress Models

Based on (1) and (2), the transferred power for each operating mode can be obtained, as given in Table II. The normalized transferred power P_o is defined as $P_o=P/P_N$, where $P_N=V_1V_2T_{hs}/(4nL_s)$. Furthermore, the peak current for a certain operating mode is related to the ranges of the voltage conversion ratio k, since the current slopes during different intervals are determined by the two transformer terminal voltages v_{ab} and v_{cd}, as shown in (1). The normalized peak current i_o for each mode under all ranges of k can be calculated, as given in Table III, where i_o is defined as $i_o=i_{pk}/I_N$ with i_{pk} being the peak current. According to the models of the transferred power and peak current, as well as the ZVS constraints, the optimal control strategy to reduce the current stress and achieve ZVS can be developed, which is detailed in the next section.

III. OPTIMAL CONTROL STRATEGY

A. Optimization Problem

The optimization problem is to explore the optimum combinations of the control variables $(D_1^*, D_2^*, D_0^*, D^*)$, which can achieve the ZVS constraints for certain operating modes and can minimize the current stress during the entire power range. That is, the current stress minimization is the optimization objective, and the ZVS constraints, mode constraints (as shown in Fig. 3), and reference power are the optimal constraints, which should be satisfied during the calculations.

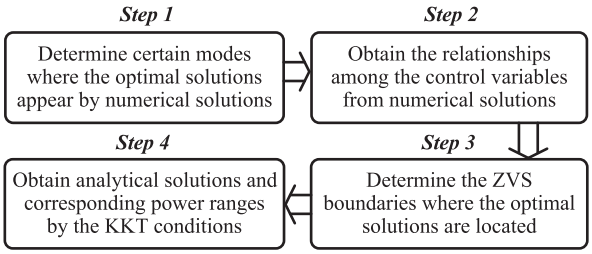

Fig. 4. Calculation process for obtaining analytical solutions.

The KKT is a general method to the analytical solutions for such an optimization problem with inequality constraints, which can be expressed as

$$\begin{cases} E(\boldsymbol{X},\lambda,\mu_m)=i_0(\boldsymbol{X})+\lambda(P_0(\boldsymbol{X})-P_0^*)+\sum_{m=1}\mu_m f_m(\boldsymbol{X}) \\ \left.\frac{\partial E}{\partial \boldsymbol{X}}\right|_{X=X^*}=0 \\ \mu_m f_m(\boldsymbol{X}^*)=0, f_m(\boldsymbol{X}^*)\le 0, \lambda\ne 0, \mu_m\ge 0 \end{cases} \tag{7}$$

in which $E(\boldsymbol{X},\lambda,\mu_m)$ is the Lagrangian function, $\boldsymbol{X}^*$ is the optimum combination of the control variables, λ and μ_m are the KKT multipliers, and $f_m(\boldsymbol{X})$ is the set of all the constraints, including the ZVS constraints and operating mode constraints. It can be seen from Table I that there are two thresholds in the ZVS constraints, i.e., I_{ZVS1} and I_{ZVS2}. In order to simplify the calculations, the larger value is applied to calculate the optimal solutions, i.e.,

$$I_{\text{ZVS}}=\max\left\{\frac{I_{\text{ZVS1}}}{I_N},\frac{I_{\text{ZVS2}}}{I_N}\right\}. \tag{8}$$

As the threshold I_{ZVS} is generally close to 0 due to the low output capacitance, certain prior-art work replaced it by 0 [24], [27]. By doing so, the calculations for analytical solutions can be simplified. However, certain switches cannot operate in ZVS in practice, since part of the instantaneous inductor currents at the rising edges of the gate pulses will be equal to 0, which fails to provide a required discharging path for the output capacitors. This condition is defined as quasi-ZVS condition. On the other hand, the condition with the I_{ZVS} obtained by (6) and (8) (i.e., $I_{\text{ZVS}}\ne 0$) is defined as strict-ZVS condition hereafter.

B. Analytical Solutions During Quasi-ZVS Operation

Due to the complex constraints and different operating modes, obtaining the analytical solutions by directly using the KKT conditions is challenging. Therefore, the optimal numerical solutions are applied to determine certain modes where the minimum current stresses are located, and also identify the ZVS boundaries in a certain mode to simplify the constraints to some extent. Then, the analytical solutions can be obtained based on the simplified KKT conditions. The entire process to simplify the calculations of the analytical solutions is shown in Fig. 4, which is detailed in the following.

Step 1: Fig. 5 illustrates the minimum current stresses for each operating mode under quasi-ZVS operation during $0.5<k\le 1$, which are obtained using Mathematica. It can be seen

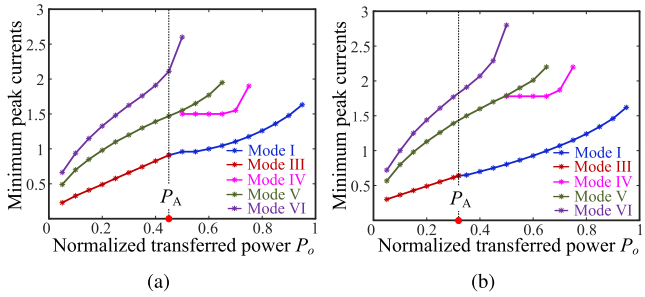

Fig. 5. Minimum current stresses for each operating mode when: (a) $k=0.6$ and (b) $k=0.8$ under quasi-ZVS operation.

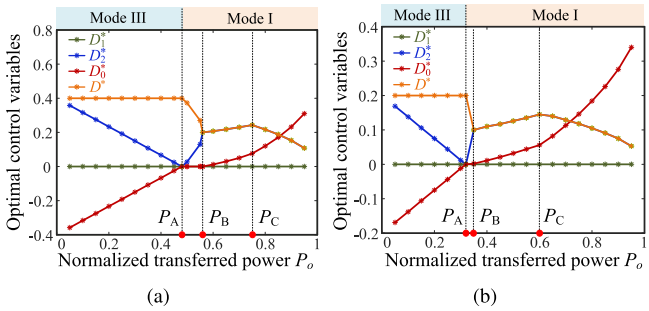

Fig. 6. Optimal control variables when: (a) $k=0.6$ and (b) $k=0.8$ under quasi-ZVS operation, where the expressions of the control variables are different during the four power ranges divided by the three power boundaries P_{A}, P_{B}, and P_{C}.

in Fig. 5 that for different operating modes, the transferred power will overlap under certain operating range. The minimum current stresses for Modes I and III are lower than those of the other three modes during the entire power range. Hence, the optimal solutions are located at Modes I and III during $P_{\text{A}}<P_o\le 1$ and $0<P_o\le P_{\text{A}}$, respectively. Thus, the analytical solutions of the other three modes (i.e., Modes IV–VI) are not considered, since they will not contribute to the MCS control.

Step 2: Fig. 6 shows the corresponding optimal control variables D_1^*, D_2^*, D_0^*, and D^* of Modes I and III. From the numerical solutions, certain relationships of the control variables can be obtained as

$$\begin{cases} \text{Mode III } (P_o\le P_{\text{A}}): D_1^*=0, D^*=1-k, D_0^*=-D_2^* \\ \text{Mode I} \begin{cases} P_{\text{A}}<P_o\le P_{\text{B}}: D_1^*=D_0^*=0 \\ P_{\text{B}}<P_o\le 1: \quad D_1^*=0, D_2^*=D^*. \end{cases} \end{cases} \tag{9}$$

Step 3: With the above relationships for Mode III (i.e., $0<P_o\le P_{\text{A}}$), the optimal analytical solution for D_2^* can be obtained as

$$D_2^*=1-k-\frac{P_o}{2k}. \tag{10}$$

Thus, the expressions of the four control variables can be obtained. On the other hand, as for Mode I, two power ranges are divided according to different relationships, i.e., $P_{\text{A}}<P_o\le P_{\text{B}}$ and $P_{\text{B}}<P_o\le 1$, as shown in (9). Furthermore, D_2^* and D^* will increase along with the transferred power during $P_{\text{B}}<$

TABLE IV
ANALYTICAL SOLUTIONS FOR MINIMIZING CURRENT STRESS UNDER QUASI-ZVS CONTROL

Range of k	Range of P_o	Analytical solutions
$k>1$	$2\frac{k-1}{k^2}<P_o\le 1$	$D_1=(k-1)\sqrt{\frac{1-P_o}{k^2-2k+2}}$, $D_0=\frac{(2-k)D_1-k+1}{2(1-k)}$, $D_2=D=0$
	$0<P_o\le 2\frac{k-1}{k^2}$	$D_1=1-\sqrt{\frac{P_o}{2(k-1)}}$, $D_2=0$, $D_0=(k-1)(1-D_1)$, $D=1-k+kD_1$
$0.5<k\le 1$	$\frac{k^4-7k^2+4k+2}{(2-k^2)^2}<P_o\le 1$	$D_2=(1-k)\sqrt{\frac{1-P_o}{3k^2-4k+2}}$, $D_0=\frac{(k-2)D_2}{2(1-k)}+\frac{1}{2}$, $D_1=0$, $D=D_2$
	$\frac{-3k^2+2k+1}{2}<P_o\le\frac{k^4-7k^2+4k+2}{(2-k^2)^2}$	$D_2=\frac{2k+2-\sqrt{6k^4+8k^3+2k^2-2(3k^4+4k^3+2k^2)P_o}}{2(3k^2+4k+2)}$, $D_0=\frac{D_2}{k}+\frac{k-1}{2k}$, $D_1=0$, $D=D_2$
	$2k(1-k)<P_o\le\frac{-3k^2+2k+1}{2}$	$D_2=\frac{1-k-\sqrt{(1-k)^2+2(2k-2k^2-P_o)}}{2}$, $D_1=D_0=0$, $D=1-k-D_2$
	$0<P_o\le 2k(1-k)$	$D_2=1-k-\frac{P_o}{2k}$, $D_1=0$, $D=1-k$, $D_0=-D_2$
$0<k\le 0.5$	$\frac{k^4+2k^3+4k}{(k^2+k+1)^2}<P_o\le 1$	$D_2=k\sqrt{\frac{1-P_o}{3k^2-2k+1}}$, $D_1=0$, $D=\frac{1-k}{k}D_2$, $D_0=\frac{1}{2}-\frac{1+k}{2k}D_2$
	$P_{\rm D}<P_o\le\frac{k^4+2k^3+4k}{(k^2+k+1)^2}$	$D_2=\frac{(2k^3+2k^2-1)(A_2+\sqrt{A_2^2-4A_1A_3+2A_1P_o})}{2(4k^3+3k^2-1)A_1}+\frac{2k^2+k-1}{4k^3+3k^2-1}$, $D_1=0$, $D=\frac{4k^3+3k^2-1}{-2k^3-2k^2+1}D_2+\frac{2k^2+k-1}{2k^3+2k^2-1}$, $D_0=\frac{(2k^2+k)D+4k^3-k^2-k}{8k^3+6k^2-2}$
	$2k(1-k)<P_o\le P_{\rm D}$	$D_2=\frac{1-k-\sqrt{(1-k)^2+2(2k-2k^2-P_o)}}{2}$, $D_1=D_0=0$, $D=1-k-D_2$
	$0<P_o\le 2k(1-k)$	$D_2=k-\frac{P_o}{2(1-k)}$, $D_1=0$, $D=1-k$, $D_0=-\frac{D_2}{2k}$
$A_1=\frac{-48k^6-88k^5-52k^4+12k^3+18k^2-4}{(8k^3+6k^2-2)^2}$, $A_2=\frac{8k^5+12k^4+2k^3-4k^2-k+1}{(4k^3+3k^2-1)^2}$, $A_3=\frac{12k^6+24k^5+k^4-12k^3-3k^2+2k}{2(4k^3+3k^2-1)^2}$		
when $0.32<k\le 0.5$, $P_{\rm D}=\frac{-3k^2+2k+1}{2}$; when $0<k\le 0.32$, $P_{\rm D}=\frac{(2(4k^2-k-1)A_1-(2k+1)A_2)^2+(2k+1)^2(8A_1A_3-2A_2^2)}{2(2k+1)^2A_1}$		

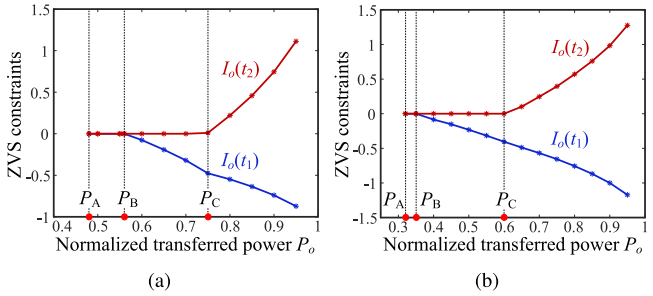

Fig. 7. Optimal control variables when: (a) $k=0.6$ and (b) $k=0.8$ under quasi-ZVS operation.

$P_o\le P_{\rm C}$, while they will decrease during $P_{\rm C}<P_o\le 1$. Thus, the analytical solutions will be different under three power ranges during Mode I, i.e., $P_{\rm A}<P_o\le P_{\rm B}$, $P_{\rm B}<P_o\le P_{\rm C}$, and $P_{\rm C}<P_o\le 1$.

The optimal solutions will appear at the boundaries of the constraints under certain conditions. For Mode I, the inductor current i_L will monotonically increase from t_0 to t_5 (see Fig. 2) during $0.5<k\le 1$. Therefore, all the ZVS constraints can be fulfilled once $I_L(t_1)\le -I_{\rm ZVS}$ and $I_L(t_2)\ge I_{\rm ZVS}$ are achieved. Fig. 7 shows the curves after substituting the obtained optimal numerical solutions for Mode I into the expressions of $I_o(t_1)$ and $I_o(t_2)$, where $I_o(t_1)=I_L(t_1)/I_N$ and $I_o(t_2)=I_L(t_2)/I_N$. As shown in Fig. 7, the optimal solutions will appear at the boundaries $I_o(t_1)=-I_{\rm ZVS}$ and $I_o(t_2)=I_{\rm ZVS}$ (note that $I_{\rm ZVS}=0$ in the quasi-ZVS operation) during $P_{\rm A}<P_o\le P_{\rm B}$, while they will appear at the boundary $I_L(t_2)=I_{\rm ZVS}$ during $P_{\rm B}<P_o\le P_{\rm C}$. On the other hand, the optimal solutions will not be affected by the ZVS constraints during $P_{\rm C}<P_o\le 1$. To sum up, the relationships among various control variables for Mode I can be obtained as

$$\begin{cases} P_{\rm A}<P_o\le P_{\rm B}: \begin{cases} D_1^*=D_0^*=0 \\ I_o(t_1)=2((k-2)D_1^*-D_2^*-2D_0^* \\ \qquad -D^*-k+1)=0 \\ I_o(t_2)=2(-kD_1^*-D_2^*+2kD_0^* \\ \qquad -D^*-k+1)=0 \end{cases} \\ P_{\rm B}<P_o\le P_{\rm C}: \begin{cases} D_1^*=0, D_2^*=D^* \\ I_o(t_2)=2(-kD_1^*-D_2^*+2kD_0^* \\ \qquad -D^*-k+1)=0 \end{cases} \\ P_{\rm C}<P_o\le 1: \quad D_1^*=0, D_2^*=D^*. \end{cases} \tag{11}$$

Step 4: By substituting (11) into (7), the calculations with the KKT conditions can be simplified, and then, the analytical solutions for Modes I and III can be obtained, as given in Table IV. Similarly, by combining the analytical solutions and all the constraints of each operating mode, the transferred power boundaries can be obtained as

$$\begin{cases} P_{\rm A}=2k(1-k) \\ P_{\rm B}=\frac{-3k^2+2k+1}{2} \\ P_{\rm C}=\frac{k^4-7k^2+4k+2}{(2-k^2)^2}. \end{cases} \tag{12}$$

So far, the analytical solutions under the entire power range during $0.5<k\le 1$ are obtained. With a similar analysis, the analytical solutions during the other two ranges of the voltage conversion ratio, i.e., $0<k\le 0.5$ and $k>1$, can also be obtained, as given in Table IV. In the obtained optimal control, Modes I and II are employed during $k>1$, while Mode I and III are used during $0<k\le 1$.

According to the above analysis, the obtained optimal solutions may occur at $I_L(t_i)=0$ and/or $I_L(t_j)=0$ under certain operating conditions. Thus, certain switches cannot achieve ZVS in practice. For instance, during $P_{\rm B}<P_o\le P_{\rm C}$ for the condition

TABLE V
SOFT-SWITCHING CONDITIONS WITH THE QUASI-ZVS CONTROL STRATEGY

Ranges of k	Ranges of P_o	Soft-switching states					
			S_{11} and S_{12}	S_{13} and S_{14}	S_{21} and S_{24}	S_{22} and S_{23}	S_{25}–S_{28}
$k>1$	$2\frac{k-1}{k^2}<P_o\le 1$	Turn ON	ZVS	ZVS	ZVS	ZVS	ZVS
		Turn OFF					
	$0<P_o\le 2\frac{k-1}{k^2}$	Turn ON	ZVS	Q-ZCS	Q-ZCS	Q-ZCS	Q-ZCS
		Turn OFF		Q-ZCS	Q-ZCS	Q-ZCS	Q-ZCS
$0.5<k\le 1$	$\frac{k^4-7k^2+4k+2}{(2-k^2)^2}<P_o\le 1$	Turn ON	ZVS	ZVS	ZVS	ZVS	ZVS
		Turn OFF					
	$\frac{-3k^2+2k+1}{2}<P_o\le\frac{k^4-7k^2+4k+2}{(2-k^2)^2}$	Turn ON	ZVS	ZVS	ZVS	Q-ZCS	ZVS
		Turn OFF			Q-ZCS		
	$0<P_o\le\frac{-3k^2+2k+1}{2}$	Turn ON	Q-ZCS	Q-ZCS	ZVS	Q-ZCS	ZVS
		Turn OFF	Q-ZCS	Q-ZCS	Q-ZCS		
$0<k\le 0.5$	$\frac{k^4+2k^3+4k}{(k^2+k+1)^2}<P_o\le 1$	Turn ON	ZVS	ZVS	ZVS	ZVS	ZVS
		Turn OFF					
	$P_{\rm D}<P_o\le\frac{k^4+2k^3+4k}{(k^2+k+1)^2}$	Turn ON	ZVS	ZVS	ZVS	Q-ZCS	ZVS
		Turn OFF			Q-ZCS		
	$0<P_o\le P_{\rm D}$	Turn ON	Q-ZCS	Q-ZCS	ZVS	Q-ZCS	ZVS
		Turn OFF	Q-ZCS	Q-ZCS	Q-ZCS		

TABLE VI
ANALYTICAL SOLUTIONS FOR MINIMIZING CURRENT STRESS UNDER STRICT-ZVS CONTROL DURING $0.5<K\le 1$

Range of P_o	Analytical solutions
$1-\frac{(3k^2-4k+2)(1-I_{\rm ZVS})^2}{(2-k^2)^2}<P_o\le 1$	$D_2=(1-k)\sqrt{\frac{1-P_o}{3k^2-4k+2}}$, $D_0=\frac{(k-2)D_2}{2(1-k)}+\frac{1}{2}$, $D_1=0$, $D=D_2$
$\frac{A_4}{2(k+1)^2}<P_o\le 1-\frac{(3k^2-4k+2)(1-I_{\rm ZVS})^2}{(2-k^2)^2}$	$D_2=\frac{(2k+2)(1-I_{\rm ZVS})-\sqrt{A_5}}{2(3k^2+4k+2)}$, $D_0=\frac{D_2}{k}+\frac{k-1+I_{\rm ZVS}}{2k}$, $D_1=0$, $D=D_2$
$P_{\rm E}<P_o\le\frac{A_4}{2(k+1)^2}$	$D_2=\frac{(1-k)(k+1-I_{\rm ZVS})-\sqrt{A_4-2(k+1)^2}}{2(k+1)}$, $D_1=0, D_0=\frac{I_{\rm ZVS}}{k+1}$, $D=1-k+\frac{(k+1)I_{\rm ZVS}}{k+1}-D_2$
$0<P_o\le 2(k-I_{\rm ZVS})(1-k+I_{\rm ZVS}-\frac{2I_{\rm ZVS}}{k})$	$D_2=\frac{-k^2+(1+I_{\rm ZVS})k-2I_{\rm ZVS}}{k}-\frac{P_o}{2(k-I_{\rm ZVS})}$, $D_1=0$, $D=1-k+I_{\rm ZVS}$, $D_0=-\frac{I_{\rm ZVS}}{k}-D_2$

$$A_4=-3k^4+(6I_{\rm ZVS}-4)k^3+(2-3I_{\rm ZVS}^2+6I_{\rm ZVS})k^2+(4-2I_{\rm ZVS}^2+2I_{\rm ZVS})k-3I_{\rm ZVS}^2+2I_{\rm ZVS}+1$$

$$A_5=4(1+k^2)(1-I_{\rm ZVS})^2+(6k^2+8k+4)(k^2+2I_{\rm ZVS}-I_{\rm ZVS}^2-1-k^2P_o)$$

$$P_{\rm E}=2\frac{-k^4+(2I_{\rm ZVS}-1)k^3+(1-I_{\rm ZVS}^2+I_{\rm ZVS})k^2+k-I_{\rm ZVS}^2+I_{\rm ZVS}}{(k+1)^2}$$

of $0.5<k\le 1$, $I_L(t_2)=0$ is fulfilled, and thus, S_{22} and S_{23} cannot achieve ZVS due to the lack of current conduction path for discharging the output capacitors. Instead, they will be turned ON in zero-current-switching (ZCS) since the inductor current is 0 at the turn-ON instants in ideal operation. In addition, the inductor current is also 0 at the turn-OFF instants of S_{21} and S_{24} when $I_L(t_2)=0$. Thus, S_{21} and S_{24} will be turned OFF in ZCS in the ideal state. However, due to the dead time, the inductor currents at the turn-ON/OFF instants may not be equal to 0. Therefore, the strict ZCS-ON/OFF cannot be realized in certain conditions. Nevertheless, since the inductor currents at the turn-ON/OFF instants are close to 0, the switching losses will be limited [defined as quasi-ZCS (Q-ZCS)]. Therefore, the entire switching losses can still be effectively suppressed. The soft-switching conditions with the quasi-ZVS control strategy under all operating conditions are summarized in Table V.

C. Analytical Solutions During Strict-ZVS Operation

To compare the performances between the quasi-ZVS control and strict-ZVS control strategies, the analytical solutions for the strict-ZVS condition should also be obtained. In the strict-ZVS control strategy, the threshold $I_{\rm ZVS}$ is set based on (6) and (8). According to the above analysis, Modes I and II have the advantages of low current stresses during $k>1$, while Modes I and III can be applied to minimize peak currents during $k\le 1$. Therefore, the strict-ZVS control strategy still employs these three operating modes to obtain the optimal control variables. The calculation process for the analytical solutions is similar to that of the quasi-ZVS control. However, due to the additional factor $I_{\rm ZVS}$, the expressions of the control variables and power boundaries will be more complicated, as given in Table VI, where the condition of $0.5<k\le 1$ is taken as an example.

IV. COMPARISON AND CLOSED-LOOP CONTROL

A. Comparison Between Quasi-ZVS and Strict-ZVS Control

Due to different determination of $I_{\rm ZVS}$ in the quasi-ZVS control and strict-ZVS control strategies, the characteristics of the 2/3-level DAB converter with the two control strategies will also

TABLE VII
POWER RANGES WITH THE QUASI-ZVS CONTROL AND STRICT-ZVS CONTROL STRATEGIES

Range of k	Modes	Range of P_o	
		Quasi-ZVS control	Strict-ZVS control
$k>1$	Mode I	$2\frac{k-1}{k^2} < P_o \le 1$	$\frac{(2I_{ZVS})k^3-(I_{ZVS}^2+4I_{ZVS}+2)k^2+(2I_{ZVS}^2+4I_{ZVS})k-2I_{ZVS}^2}{k^4} < P_o \le 1$
	Mode II	$0 < P_o \le 2\frac{k-1}{k^2}$	$0 < P_o \le 2\frac{(2I_{ZVS}^2-3I_{ZVS}+1)k^2+(2-3I_{ZVS})(1-I_{ZVS})k-(1-I_{ZVS})^2}{k^2(k-1)}$
$k\le 1$	Mode I	$2k(1-k) < P_o \le 1$	$2\frac{-k^4+(2I_{ZVS}-1)k^3+(1-I_{ZVS}^2+I_{ZVS})k^2+k-I_{ZVS}^2+I_{ZVS}}{(k+1)^2} < P_o \le 1$
	Mode III	$0 < P_o \le 2k(1-k)$	$0 < P_o \le 2(k-I_{ZVS})(1-k+I_{ZVS}-\frac{2I_{ZVS}}{k})$

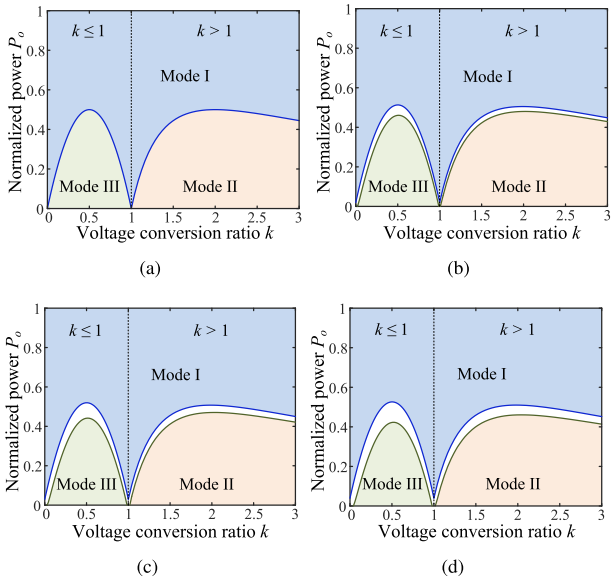

Fig. 8. Transferred power range with the strict-ZVS control when: (a) $I_{ZVS} = 0$ (quasi-ZVS), (b) $I_{ZVS} = 0.01$, (c) $I_{ZVS} = 0.015$, and (d) $I_{ZVS} = 0.02$.

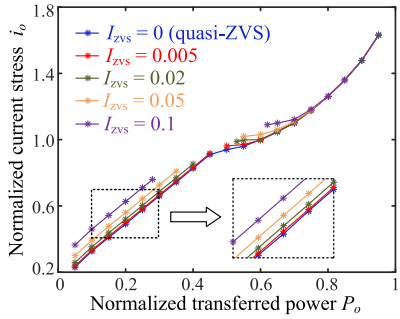

Fig. 9. Minimum current stresses with the quasi-ZVS and strict-ZVS control strategies under $k = 0.6$.

be different in terms of transferred power ranges, soft-switching regions, current stresses, and implementation complexity.

1) Transferred power ranges: The transferred power ranges of the DAB converter with the quasi-ZVS control and strict-ZVS control are summarized in Table VII, where it can be seen that the analytical solutions in the quasi-ZVS control strategy can cover the entire power range (i.e., $0 < P_o \le 1$). On the other hand, for the strict-ZVS control strategy, there will be a gap between the power ranges of the two modes, i.e., Modes I and II during $k > 1$, and Modes I and III during $k \le 1$. Fig. 8 shows the transferred power ranges with different I_{ZVS}, where it can be seen that the gap between the two modes will increase along with the values of I_{ZVS}.

2) Soft-switching regions: Table V tabulates the soft-switching condition of the quasi-ZVS control strategy. Although certain switches cannot operate in ZVS-ON, Q-ZCS-ON/OFF can also effectively reduce the switching losses. On the other hand, for the strict-ZVS control, all the switches can operate in ZVS in the corresponding regions, i.e., the colored areas in Fig. 8(b)–(d).

3) Current stresses: When considering the threshold I_{ZVS} (i.e., $I_{ZVS} \neq 0$) in the strict-ZVS control strategy, the feasible region for minimizing the current stress will be reduced compared with that of the quasi-ZVS control. Thus, the minimum current stresses obtained in the strict-ZVS control will be slightly increased. For instance, Fig. 9 shows a comparison of the minimum current stresses between the quasi-ZVS control and strict-ZVS control with various I_{ZVS} under $k = 0.6$. It can be seen in Fig. 9 that during the low power ranges, the current stresses in the strict-ZVS control are higher than those in the quasi-ZVS control, and the current stresses will be increased along with I_{ZVS}.

4) Implementation complexity: Compared with the quasi-ZVS control, the implementation complexity will be increased for the strict-ZVS control due to two reasons: 1) the expressions of the control variables and power boundaries are more complex, which makes the closed-loop control structure more difficult to design; 2) due to the gap between the two operating modes in the strict-ZVS control strategy [see Fig. 8(b)–(d)], another control strategy should be applied under those conditions to achieve continuous operation in the entire power range. However, since the control variables may not be continuous at the boundaries between the strict-ZVS control and the other control strategy, the closed-loop control system, which can achieve smooth transition between the two control strategies will be more complicated. Therefore, although the analytical solutions with the strict-ZVS conditions are able to be obtained, it is still challenging to achieve the closed-loop control.

By comprehensively considering the above characteristics, the quasi-ZVS control is more feasible in practice, especially when the operating conditions/parameters change in a wide range. On the other hand, the strict-ZVS control can be applied when the operating parameters change in a limited range with numerical solutions.

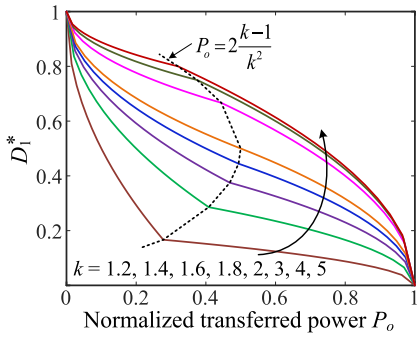

Fig. 10. Optimal phase-shift ratio D_1^* under the quasi-ZVS control for the condition of $k > 1$.

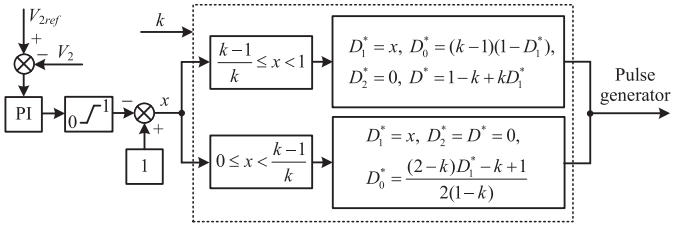

Fig. 11. Closed-loop control structure of the proposed quasi-ZVS control strategy when $k > 1$.

B. Closed-Loop Control

The closed-loop control structure for the proposed quasi-ZVS control strategy can be designed based on the analytical solutions in Table IV. However, since the transferred power should be detected online to identify certain operating mode and corresponding optimal solutions, the two-side dc voltages and currents should be detected. To reduce the sensors and the implementation complexity, a simplified closed-loop control structure is proposed.

1) Closed-loop structure for $k > 1$: D_1^* will be monotonically decreased along with the transferred power during the entire power range for $k > 1$, as shown in Fig. 10. In addition, D_1^* is continuous at the boundary of Modes I and II, i.e., $P_o = 2\frac{k-1}{k^2}$. Therefore, D_1^* is taken as the output (i.e., x) of a proportional–integral (PI) controller, i.e., $D_1^* = x$ (see Fig. 11). Since the expressions of control variables are different in the two operating modes, the value of x at the power boundary $P_o = 2\frac{k-1}{k^2}$ should be calculated as

$$x\Big|_{P_o = 2\frac{k-1}{k^2}} = \frac{k-1}{k}. \tag{13}$$

Thus, the two operating modes can be divided based on the ranges of x, i.e., Mode II for $\frac{k-1}{k} \le x < 1$, and Mode I for $0 \le x < \frac{k-1}{k}$. Accordingly, the closed-loop control structure can be designed, as shown in Fig. 11. By doing so, current sensors are not required for determining the transferred power, since the power ranges where the two modes are applied can be determined by the ranges of x.

2) Closed-loop structure for $k \le 1$: Different from the condition of $k > 1$, there is no control variable, which monotonically increases/decreases along with the transferred power.

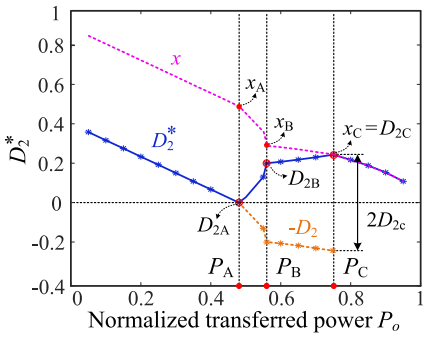

Fig. 12. Optimal control variable D_2^* when $k = 0.6$.

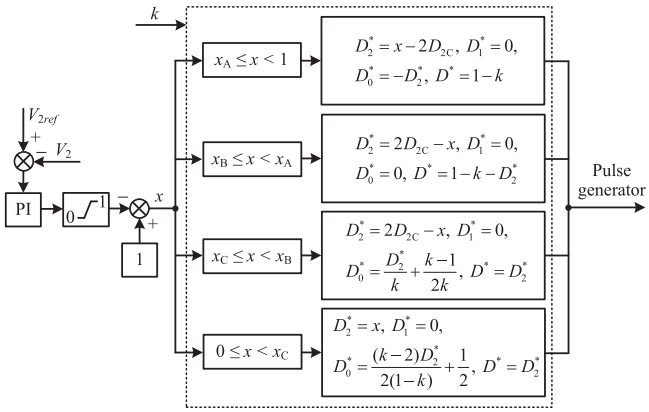

Fig. 13. Closed-loop control structure of the proposed quasi-ZVS control strategy when $0.5 < k \le 1$.

Therefore, x should be designed to meet this (i.e., x can be monotonically changed along with the transferred power) based on the optimal control variables. In Fig. 12, the blue solid line is the curve of D_2^* under the condition of $k = 0.6$, and x can be obtained as

$$x = \begin{cases} D_2^* + 2D_{2\,\mathrm{C}}, & 0 < P_o \le P_\mathrm{A} \\ -D_2^* + 2D_{2\,\mathrm{C}}, & P_\mathrm{A} < P_o \le P_\mathrm{C} \\ D_2^*, & P_\mathrm{C} < P_o \le 1 \end{cases} \tag{14}$$

where $D_{2\,\mathrm{C}}$ is the value of D_2 at the power boundary P_C, which can be obtained as

$$D_{2\,\mathrm{C}}\Big|_{P_o = P_\mathrm{C}} = \frac{1-k}{2-k^2}. \tag{15}$$

Then, x will monotonically decrease along with the transferred power, which can be seen in Fig. 12. The values of x at the three power boundaries, i.e., P_A, P_B, and P_C, can be obtained as

$$\begin{cases} x_\mathrm{A} = \frac{2(1-k)}{2-k^2} \\ x_\mathrm{B} = \frac{(1-k)(2+k^2)}{2(2-k^2)} \\ x_\mathrm{C} = \frac{1-k}{2-k^2}. \end{cases} \tag{16}$$

Then, the transferred power ranges can be converted to the ranges of x, and the closed-loop control structure when $0.5 < k \le 1$ is shown in Fig. 13, and that in the condition of $0 < k \le 0.5$ can be designed similarly.

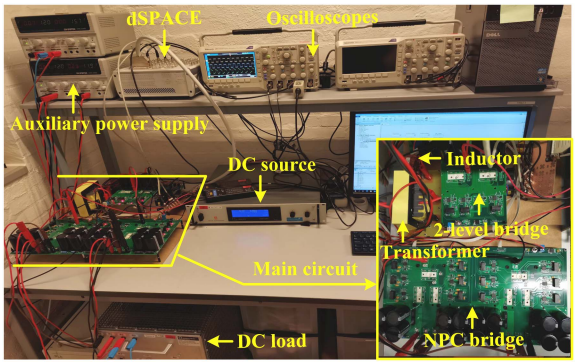

Fig. 14. 2/3-level DAB converter prototype.

TABLE VIII
MAIN PARAMETERS OF THE EXPERIMENTAL PROTOTYPE

Parameters	Values
Power rating P	2.5 kW
Transformer turns ratio n	2
Series inductor L_s	100 μH
DC-link capacitors C_1, C_2, and C_3	680 μF
Switching frequency f_s	10 kHz
Power switches (IGBT)	Semikron SK35GB12T4

V. EXPERIMENTAL VERIFICATION

Experimental tests are performed to validate the performances of the proposed control strategy, which are carried out on a down-scaled 2/3-level DAB converter prototype, as shown in Fig. 14. Key parameters of the 2/3-level DAB converter system are given in Table VIII.

Fig. 15 shows the experimental results of v_{ab}, v_{cd}, and i_L with traditional single-phase-shift (SPS) control, MCS control in [22], strict-ZVS control (with numerical solutions), and the proposed quasi-ZVS control strategies, where the input and output voltages are 200 and 300 V (i.e., $k = 1.33$), respectively, and the transferred power is 390 W. It should be noted that during $k > 1$, the optimal solutions between the MCS control and quasi-ZVS control strategies are the same. As shown in Fig. 15, the peak currents are 10.8, 9.8, and 9.6 A for the SPS control, strict-ZVS control, and MCS/quasi-ZVS control, respectively. Compared with the SPS control, the MPS control strategies (i.e., the other three control strategies) can reduce the current stress. In addition, the current stress under the quasi-ZVS/MCS control is further reduced compared with that of the strict-ZVS control. The soft-switching conditions under different control strategies can be seen from the waveforms of collector-emitter and gate-emitter voltages (i.e., v_{ce} and v_{ge}) and inductor current, as shown in Fig. 16. It can be seen in Fig. 16(a) that the switches of the NPC bridge will be turned ON in hard-switching (HS) with the SPS control. As for the strict-ZVS control, all the switches can be turned ON in ZVS. Furthermore, the switches can be turned ON in ZVS or Q-ZCS with the quasi-ZVS/MCS control strategy, and part switched can be turned OFF in Q-ZCS. The efficiency of the DAB converter with the above control strategies are obtained by a power analyzer, which is shown in Fig. 15 (i.e., $\eta = 85.8\%$ for the SPS control, 91.2% for the strict-ZVS control, and 92.3% for the quasi-ZVS/MCS control). The quasi-ZVS/MCS control can achieve higher efficiency compared with the SPS and strict-ZVS control.

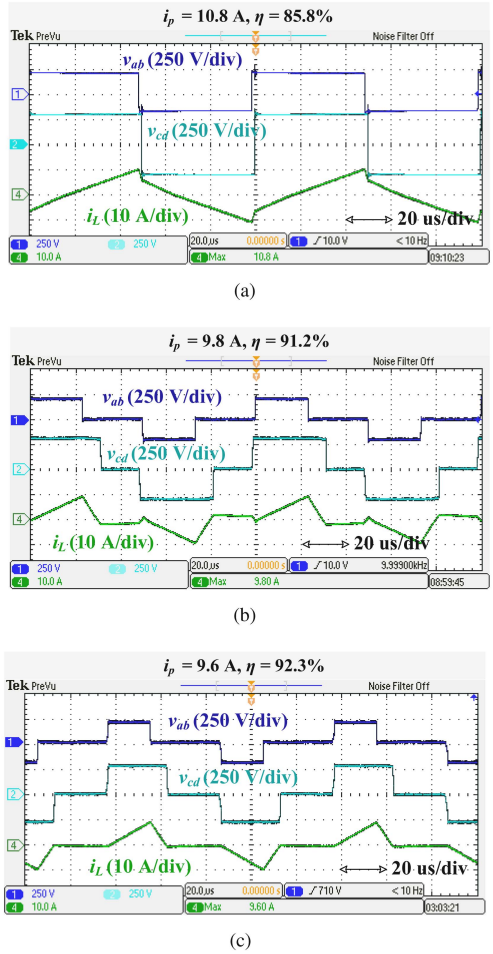

Fig. 15. Experimental results for the condition of $V_1 = 200$ V, $V_2 = 300$ V ($k = 1.33$), and $P = 390$ W with: (a) SPS control, (b) strict-ZVS control, and (c) MCS control and quasi-ZVS control.

Figs. 17 and 18 illustrate the experimental results among various control strategies for the condition of $V_1 = 90$ V, $V_2 = 300$ V (i.e., $k = 0.6$), and $P = 780$ W. It can be seen in Fig. 17 that the MCS control in [22] can achieve the lowest peak current, since the ZVS constraints are not considered during the optimization, which means the feasible region for minimizing the peak current is larger than that of the quasi-ZVS and strict-ZVS control strategies. However, as part of the switches cannot operate in soft-switching, as shown in Fig. 18, the efficiency with the MCS control is lower than that of the quasi-ZVS and strict-ZVS control strategies. On the other hand, the quasi-ZVS control can achieve the highest efficiency among different control strategies. The corresponding power loss distribution with various control strategies is shown in Fig. 19, where ET1 and ET2 denote the simulation with the operating conditions of Figs. 15 (i.e., $V_1 = 200$ V, $V_2 = 300$ V, and $P = 390$ W) and 17 (i.e., $V_1 = 90$ V, $V_2 = 300$ V, and $P = 780$ W), respectively. After comparing Fig. 19 to Figs. 15 and 17, it can be seen that the

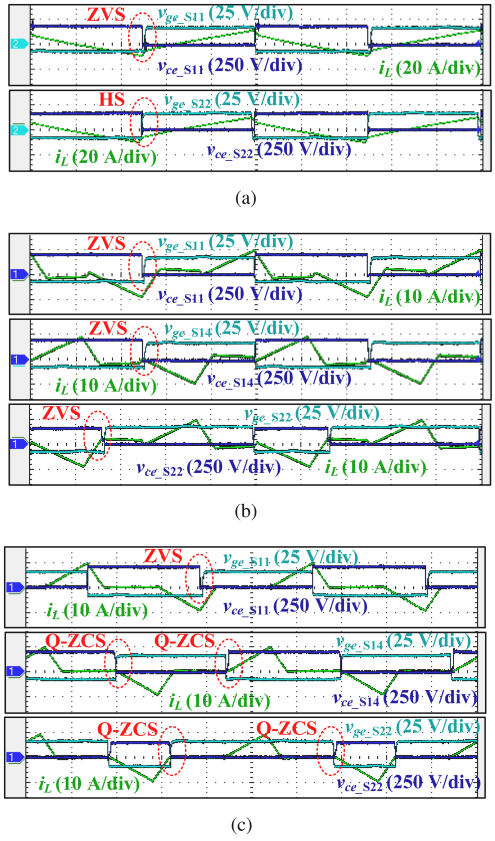

Fig. 16. Soft-switching results for the condition of $V_1 = 200$ V, $V_2 = 300$ V ($k = 1.33$), and $P = 390$ W with: (a) SPS control, (b) strict-ZVS control, and (c) MCS control and quasi-ZVS control.

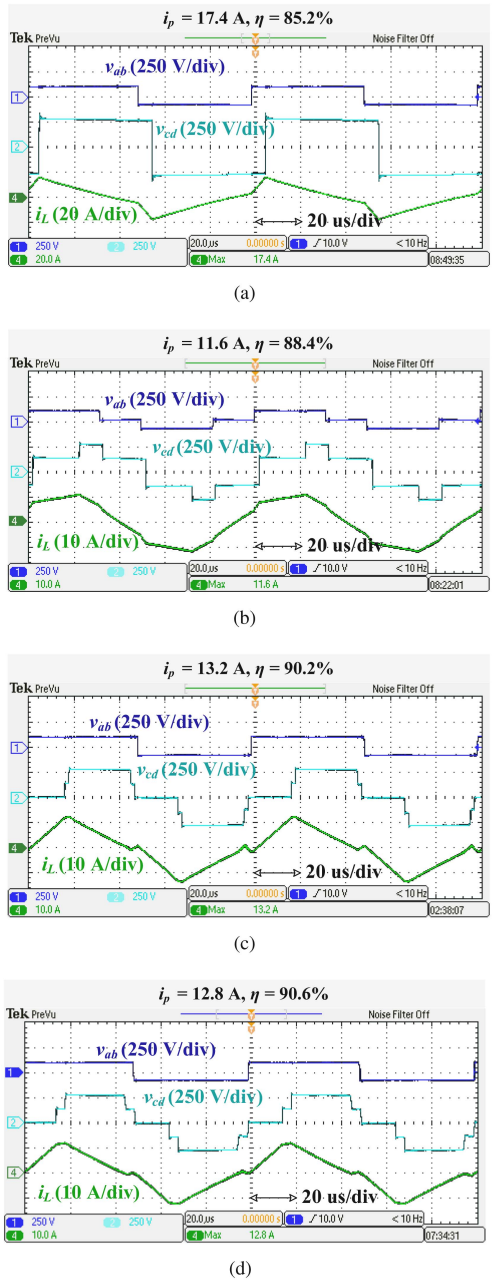

Fig. 17. Experimental results for the condition of $V_1 = 90$ V, $V_2 = 300$ V ($k = 0.6$), and $P = 780$ W with: (a) SPS control, (b) MCS control, (c) strict-ZVS control, and (d) quasi-ZVS control.

efficiency in simulation and experimental tests is close. For instance, the total power losses for SPS control is 110 W in ET2, which means the efficiency is 85.9% in simulation, and the corresponding experimental efficiency is 85.2% [see Fig. 17(a)] Furthermore, as shown in Fig. 19, compared with the other three control strategies, the entire power losses can be reduced by the quasi-ZVS control, and thus, the efficiency of the DAB converter can be enhanced.

Figs. 20 and 21 show the comparative curves in terms of the peak currents and efficiency with different control strategies under various power levels and input voltages, including the SPS control, triple-phase-shift (TPS) control in [15], MCS control, strict-ZVS control, and quasi-ZVS control. It can be seen in Figs. 20 and 21 that the MCS control can achieve the minimum peak currents among various control strategies. However, the proposed quasi-ZVS control can further improve the efficiency compared to the other strategies due to taking soft-switching into the optimization. It should be noted that the current stress and efficiency with the TPS control, MCS control, and quasi-ZVS control is identical when $k > 1$ due to the same optimal control variables. Furthermore, compared with the strict-ZVS control, another advantage of the proposed quasi-ZVS control is that the implementation can be simplified since it does not require the precalculation of the numerical solutions. It should be noted that the experimental tests are carried out in an IGBT-based prototype, while the performances of the quasi-ZVS control and strict-ZVS control strategies in the MOSFET-based prototypes have not been verified. Since the turn-ON losses are generally dominant for the MOSFET devices, the strict-ZVS control may achieve higher efficiency compared to the quasi-ZVS control in certain operating conditions. However, since the implementation complexity of the strict-ZVS control increases significantly, it can be applied only when the operating parameters change in a limited range with the precalculation of numerical solutions. Otherwise, the quasi-ZVS control is still suitably applied after compromising the efficiency and implementation complexity.

Accordingly, Fig. 22 illustrates the dynamics of the converter to verify the performances of the proposed closed-loop control

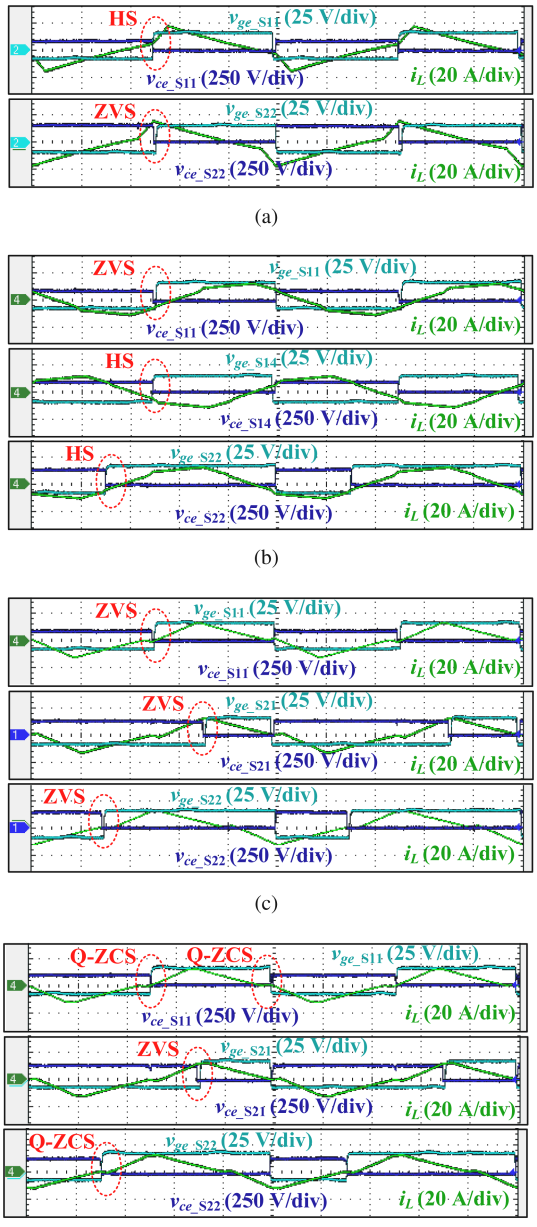

Fig. 18. Soft-switching results for the condition of $V_1 = 90$ V, $V_2 = 300$ V ($k = 0.6$), and $P = 780$ W with: (a) SPS control, (b) MCS control, (c) strict-ZVS control, and (d) quasi-ZVS control.

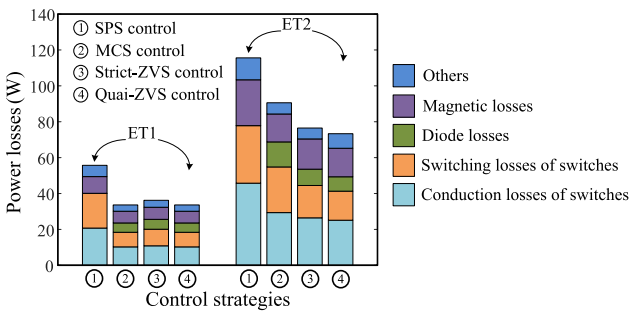

Fig. 19. Power loss distribution (simulation) of the DAB converter with various control strategies.

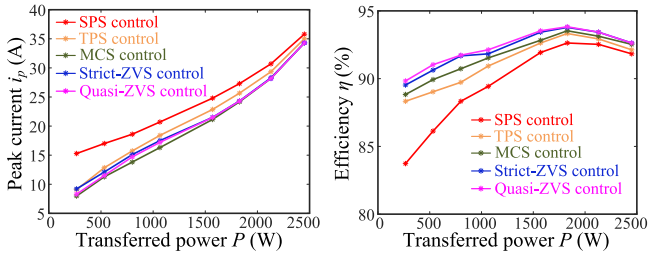

Fig. 20. Experimental comparison of different control strategies under various transferred power levels for the condition of $V_1 = 120$ V and $V_2 = 350$ V in terms of: (a) current stress and (b) efficiency.

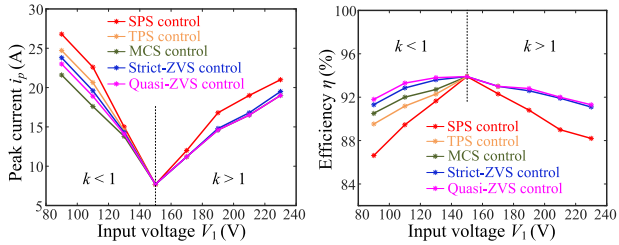

Fig. 21. Experimental comparison of different control strategies under various input voltages for the condition of $V_2 = 300$ V and $P = 1000$ W in terms of: (a) current stress and (b) efficiency.

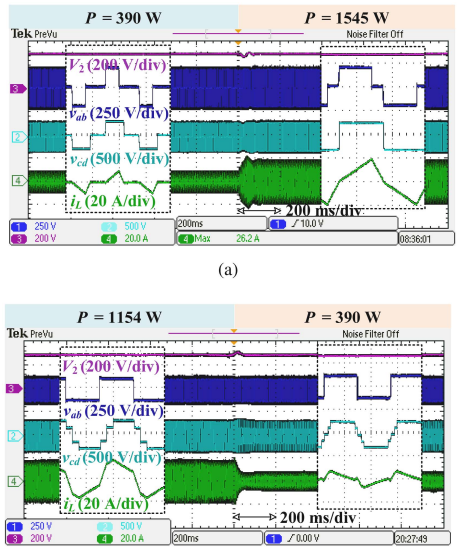

Fig. 22. Dynamic test results of the system under a step change in the transferred power with the proposed quasi-ZVS control strategy: (a) $V_1 = 200$ V, $V_2 = 300$ V (i.e., $k = 1.33$), and P changes from 390 W to 1545 W, and (b) $V_1 = 120$ V, $V_2 = 300$ V (i.e., $k = 0.8$), and P changes from 1154 to 390 W.

structure for the quasi-ZVS control. In Fig. 22(a), the transferred power is changed from 390 to 1545 W under the condition of $k = 1.33$, and in Fig. 22(b), the power is changed from 1154 to 390 W when $k = 0.8$. It can be seen in Fig. 22 that the proposed closed-loop control structure for the quasi-ZVS control can achieve smooth transition between different power ranges and operating modes under various voltage conversion ratios.

VI. Conclusion

This article has proposed an optimal control strategy for the 2/3-level DAB converter to achieve both soft-switching and MCS simultaneously. The operating modes, which are able to realize ZVS for all the switches, were discussed, and then, the ZVS constraints, transferred power and current stress models for these operating modes were obtained. Based on the above, the optimization problem, considering both the ZVS constraints and MCS, were developed. The analytical solutions for the control variables were calculated by the KKT conditions, where the calculations were simplified by a numerical solution analysis. In addition, the performances of the quasi-ZVS control and strict-ZVS control strategies were compared in terms of soft-switching regions, current stresses, implementation complexity, and efficiency. Finally, the performances of the proposed control strategy were validated by experimental tests.

References

[1] R. M. Burkart and J. W. Kolar, "Comparative $\eta-\rho-\sigma$ Pareto optimization of Si and SiC multilevel dual-active-bridge topologies with wide input voltage range," *IEEE Trans. Power Electron.*, vol. 32, no. 7, pp. 5258–5270, Jul. 2017.

[2] P. Liu, C. Chen, S. Duan, and W. Zhu, "Dual phase-shifted modulation strategy for the three-level dual active bridge DC–DC converter," *IEEE Trans. Ind. Electron.*, vol. 64, no. 10, pp. 7819–7830, Oct. 2017.

[3] C. Song, A. Sangwongwanich, Y. Yang, and F. Blaabjerg, "Capacitor voltage balancing for multi-level dual-active-bridge DC-DC converters," *IEEE Trans. Ind. Electron.*, vol. 70, no. 3, pp. 2566–2575, Mar. 2023.

[4] M. A. Moonem and H. Krishnaswami, "Analysis and control of multi-level dual active bridge DC–DC converter," in *Proc. IEEE Energy Convers. Congr. Expo.*, 2012, pp. 1556–1561.

[5] A. Filba-Martinez, S. Busquets-Monge, J. Nicolas-Apruzzese, and J. Bordonau, "Operating principle and performance optimization of a three-level NPC dual-active-bridge DC–DC converter," *IEEE Trans. Ind. Electron.*, vol. 63, no. 2, pp. 678–690, Feb. 2016.

[6] C. Song, A. Sangwongwanich, Y. Yang, and F. Blaabjerg, "A model-free capacitor voltage balancing method for multi-level DAB converters," *IEEE Trans. Power Electron.*, vol. 38, no. 1, pp. 79–84, Jan. 2023.

[7] C. Song, A. Sangwongwanich, Y. Yang, and F. Blaabjerg, "Open-circuit fault diagnosis and tolerant control for 2/3-Level DAB converters," *IEEE Trans. Power Electron.*, vol. 38, no. 4, pp. 5392–5410, Apr. 2023.

[8] N. Hou and Y. W. Li, "Overview and comparison of modulation and control strategies for a nonresonant single-phase dual-active-bridge DC–DC converter," *IEEE Trans. Power Electron.*, vol. 35, no. 3, pp. 3148–3172, Mar. 2020.

[9] B. Zhao, Q. Song, W. Liu, and Y. Sun, "Overview of dual-active-bridge isolated bidirectional DC–DC converter for high-frequency-link power-conversion system," *IEEE Trans. Power Electron.*, vol. 29, no. 8, pp. 4091–4106, Aug. 2014.

[10] Q. Bu, H. Wen, H. Shi, and Y. Zhu, "A comparative review of high-frequency transient DC bias current mitigation strategies in dual-active-bridge DC–DC converters under phase-shift modulations," *IEEE Trans. Ind. Appl.*, vol. 58, no. 2, pp. 2166–2182, Mar./Apr. 2022.

[11] Y. Tang et al., "Reinforcement learning based efficiency optimization scheme for the DAB DC–DC converter with triple-phase-shift modulation," *IEEE Trans. Ind. Electron.*, vol. 68, no. 8, pp. 7350–7361, Aug. 2021.

[12] Q. Gu, L. Yuan, J. Nie, J. Sun, and Z. Zhao, "Current stress minimization of dual-active-bridge DC–DC converter within the whole operating range," *IEEE J. Emerg. Sel. Topics Power Electron.*, vol. 7, no. 1, pp. 129–142, Mar. 2019.

[13] O. M. Hebala, A. A. Aboushady, K. H. Ahmed, and I. Abdelsalam, "Generic closed-loop controller for power regulation in dual active bridge DC–DC converter with current stress minimization," *IEEE Trans. Ind. Electron.*, vol. 66, no. 6, pp. 4468–4478, Jun. 2019.

[14] N. Hou, W. Song, and M. Wu, "Minimum-current-Stress scheme of dual active bridge DC–DC converter with unified phase-shift control," *IEEE Trans. Power Electron.*, vol. 31, no. 12, pp. 8552–8561, Dec. 2016.

[15] J. Huang, Y. Wang, Z. Li, and W. Lei, "Unified triple-phase-shift control to minimize current stress and achieve full soft-switching of isolated bidirectional DC–DC converter," *IEEE Trans. Ind. Electron.*, vol. 63, no. 7, pp. 4169–4179, Jul. 2016.

[16] B. Liu, P. Davari, and F. Blaabjerg, "An optimized hybrid modulation scheme for reducing conduction losses in dual active bridge converters," *IEEE J. Emerg. Sel. Topics Power Electron.*, vol. 9, no. 1, pp. 921–936, Feb. 2021.

[17] Z. Guo and X. Han, "Control strategy of AC–DC converter based on dual active bridge with minimum current stress and soft switching," *IEEE Trans. Power Electron.*, vol. 37, no. 9, pp. 10178–10189, Sep. 2022.

[18] S. Chaurasiya and B. Singh, "A load adaptive hybrid DPS control for DAB to secure minimum current stress and full ZVS operation over wide load and voltage conversion ratio," *IEEE Trans. Ind. Appl.*, vol. 59, no. 2, pp. 1901–1911, Mar./Apr. 2023.

[19] L. Shu, W. Chen, M. Shi, R. Liu, S. Gao, and F. Deng, "Improved control strategy of triple-voltage three-phase DAB (T2-DAB) converter for current stress and zero-voltage-switching optimization," *IEEE J. Emerg. Sel. Topics Power Electron.*, vol. 10, no. 1, pp. 773–784, Feb. 2022.

[20] P. Liu, C. Chen, and S. Duan, "An optimized modulation strategy for the three-level DAB converter with five control degrees of freedom," *IEEE Trans. Ind. Electron.*, vol. 67, no. 1, pp. 254–264, Jan. 2020.

[21] Y. Wang et al., "Minimum-current-Stress scheme of three-level dual-active-bridge DC–DC converters with the particle swarm optimization," *IEEE Trans. Transport. Electrific.*, vol. 7, no. 4, pp. 2067–2084, Dec. 2021.

[22] C. Song, A. Sangwongwanich, Y. Yang, Y. Pan, and F. Blaabjerg, "Analysis and optimal modulation for 2/3-Level DAB converters to minimize current stress with five-level control," *IEEE Trans. Power Electron.*, vol. 38, no. 4, pp. 4596–4612, Apr. 2023.

[23] P. Liu and S. Duan, "A ZVS range enhancement strategy for the DAB converter by using blocking capacitors," *IEEE J. Emerg. Sel. Topics Power Electron.*, vol. 9, no. 2, pp. 1389–1398, Apr. 2021.

[24] L. Jin, B. Liu, and S. Duan, "ZVS soft switching operation range analysis of three-level dual-active bridge DC–DC converter under phase shift control strategy," *IEEE Trans. Ind. Appl.*, vol. 55, no. 2, pp. 1963–1972, Mar./Apr. 2019.

[25] W. Ye, S. Shao, Q. Guo, J. Zhang, and K. Sheng, "A phase shift control of minimal circulating current and ZVS turn-on for DAB converter," in *Proc. IEEE 2nd Int. Electr. Energy Conf.*, Beijing, China, 2018, pp. 682–686.

[26] E. L. Carvalho, C. A. Felipe, L. V. Bellinaso, C. M. D. O. Stein, R. Cardoso, and L. Michels, "Asymmetrical-PWM DAB converter with extended ZVS/ZCS range and reduced circulating current for ESS applications," *IEEE Trans. Power Electron.*, vol. 36, no. 11, pp. 12990–13001, Nov. 2021.

[27] Y. Hu et al., "Efficiency evaluation for DAB converter with reactive power minimization strategy and full ZVS operation," in *Proc. IEEE Energy Convers. Congr. Expo.*, 2019, pp. 4274–4280.

Chaochao Song (Member, IEEE) received the B.S. degree in automation and M.S. degree in power electronics from Shandong University, Ji'nan, China, in 2016 and 2019, respectively, and the Ph.D. degree in energy technology from Aalborg University, Aalborg, Denmark, in 2023.

From June 2022 to September 2022, he was a Visiting Researcher with Fraunhofer ISE, Freiburg, Germany. He is currently a Postdoc with Aalborg University. His current research interests include control of DAB converters, multilevel converters, and modeling of SiC-based power electronic converters.

Ariya Sangwongwanich (Member, IEEE) received the B.Eng. degree in electrical engineering from Chulalongkorn University, Bangkok, Thailand, in 2013, and the M.Sc. and Ph.D. degrees in energy engineering from Aalborg University, Aalborg, Denmark, in 2015 and 2018, respectively.

He is currently an Assistant Professor with the Department of Energy Technology, Aalborg University, where he is also a Vice Leader of Photovoltaic Systems Research Program. In 2017, he was a Visiting Researcher with RWTH Aachen, Aachen, Germany, in 2017 and with the University of Cambridge, Cambridge, U.K., in 2023. His research interests include control of grid-connected converters, photovoltaic systems, and reliability and sustainability in power electronics.

Dr. Sangwongwanich was the recipient of the Danish Academy of Natural Sciences' Ph.D. Prize and the Spar Nord Foundation Research Award for the Ph.D. thesis in 2019.

Yongheng Yang (Senior Member, IEEE) received the B.Eng. degree in electrical engineering and automation from Northwestern Polytechnical University, Xi'an, China, in 2009, the Ph.D. degree in energy technology from Aalborg University, Aalborg, Denmark, in 2014, and the postgraduate degree from Southeast University, Nanjing, China, in 2011.

During March–May 2013, he was a Visiting Scholar with Texas A & M University, College Station, TX, USA. From 2014 to 2020, he was with the Department of Energy Technology, Aalborg University, where he was a Tenured Associate Professor in 2018. In 2021, he joined as a ZJU100 Professor with Zhejiang University, Hangzhou, China. He became a Zhejiang Kunpeng Investigator in 2023. His research interests include grid-friendly integration of photovoltaic systems and control of power converters, specifically grid-forming technologies.

Dr. Yang was the recipient of the 2018 IET Renewable Power Generation Premium Award, 2021 Richard M. Bass Outstanding Young Power Electronics Engineer Award from the IEEE Power Electronics Society (PELS), 2022 IEEJ Isao Takahashi Power Electronics Award, and three IEEE Best Paper Awards, an Outstanding Reviewer for IEEE TRANSACTIONS ON POWER ELECTRONICS in 2018. He was the Chair of IEEE Denmark Section during 2019–2020. He is an Associate Editor for several IEEE transactions. He was included on the list of the Highly Cited Chinese Researchers by Elsevier in 2022–2023. He is currently a Vice Chair of the IEEE PELS Technical Committee on Sustainable Energy Systems and a Council Member of the China Power Supply Society.

Frede Blaabjerg (Fellow, IEEE) received the Ph.D. degree in electrical engineering from Aalborg University, Aalborg, Denmark, in 1995.

From 1987 to 1988, he was with ABB-Scandia, Randers, Denmark. He became an Assistant Professor in 1992, an Associate Professor in 1996, and a Full Professor of power electronics and drives in 1998 with AAU Energy, Aalborg. In 2017, he became a Villum Investigator. He was a Honoris Causa with University Politehnica Timisoara, Timişoara, Romania, in 2017 and with Tallinn Technical University, Tallinn, Estonia, in 2018. He has authored or coauthored more than 600 journal papers in the fields of power electronics and its applications. He is the coauthor of eight monographs and the Editor of fourteen books in power electronics and its applications, e.g., the series (four volumes) *Control of Power Electronic Converters and Systems* published by Academic Press/Elsevier. His current research interests include power electronics and its applications such as in wind turbines, PV systems, reliability, power-2-X, power quality, and adjustable speed drives.

Dr. Blaabjerg was the recipient of 38 IEEE Prize Paper Awards, IEEE PELS Distinguished Service Award in 2009, EPE-PEMC Council Award in 2010, IEEE William E. Newell Power Electronics Award 2014, Villum Kann Rasmussen Research Award 2014, Global Energy Prize in 2019, and 2020 IEEE Edison Medal. From 2006 to 2012, he was an Editor-in-Chief of IEEE TRANSACTIONS ON POWER ELECTRONICS. From 2005 to 2007, he was a Distinguished Lecturer with the IEEE Power Electronics Society and with the IEEE Industry Applications Society from 2010 to 2011 as well as 2017 to 2018. During 2019–2020, he was a President of IEEE Power Electronics Society. He was the Vice-President of the Danish Academy of Technical Sciences, Kongens Lyngby, Denmark. He is nominated in 2014-2020 by Thomson Reuters to be between the most 250 cited researchers in Engineering in the world.